# Molecular dynamics study on the nano-void growth in face-centered cubic single crystal copper

K.J. Zhao [a], C.Q. Chen [a,b,*], Y.P. Shen [a], T.J. Lu [a]

[a] MOE Key Laboratory for Strength and Vibration, School of Aerospace, Xi'an Jiaotong University, Xi'an 710049, PR China
[b] AML, Department of Engineering Mechanics, Tsinghua University, Beijing 100084, PR China

ARTICLE INFO

ABSTRACT

Cylindrical nano-void growth in face-centered cubic single crystal copper is studied by mean of molecular dynamics with the Embedded Atom Method. The problem is modeled by a periodic unit cell containing a centered nano-sized cylindrical hole subject to uniaxial tension. The effects of the cell size, crystalline orientation, and initial void volume fraction on the macroscopic stress–strain curve, incipient yield strength, and macroscopic effective Young's modulus are quantified. Defect evolution in terms of dislocation emission immediately after incipient yielding is also investigated. Obtained results show that, for a given void volume fraction, cell size has apparent effects on the incipient yield strength but negligible effects on the macroscopic effective Young's modulus. Moreover, the macroscopic effective Young's modulus and incipient yield strength of the $[\bar{1}\,1\,0]$–$[1\,1\,1]$–$[1\,1\,\bar{2}]$ orientated system are found to be much more sensitive to the presence of void than those of the $[1\,0\,0]$–$[0\,1\,0]$–$[0\,0\,1]$ system.

© 2009 Elsevier B.V. All rights reserved.

## 1. Introduction

The nucleation, growth, and coalescence of voids have been commonly accepted as the prime processes responsible for the ductile failure of metals and are all crucial for the material strength. At macro-scales, ductile failure in terms of void growth has been extensively studied, leading to various continuum models (e.g., [1–7]) to quantify the void growth and to describe the mechanical behavior of metals. It is noted that at the incipient stage of void growth the size of a typical void may lie in the range of sub-microns or even nano-meters. On such small length scales, size effects are expected and attempts have been made to include the size effects into the continuum void growth models by introducing an intrinsic material length scale ([8–11]).

Another problem with continuum models is that they are not suitable for uncovering the underlying physical mechanisms for void growth. Given the currently available technologies, direct experiment observation of void growth in metals at micro or nano scale is still a formidable task, though a recent high strain rate experimental shows that dislocation emission may dominate the early states of void growth [12]. As a result, "Virtual experiments" such as micro and nano scale numerical simulations (e.g., discrete dislocation modeling, molecular dynamics simulation) are preferred for exploring the physical mechanism of void growth at small scales.

The method of discrete dislocation (DD) dynamics developed by Van der Giessen and Needleman [13] was employed by several groups to study the void growth at small scale (e.g., [14–16]). Although these DD studies are two dimensional, they demonstrated evidently size effects in the flow stress, strain hardening rate, and void growth rate, showing the features of "smaller behavior stronger" and "smaller is slower". The Molecular dynamics (MD) method when compared to the DD dynamics method has the advantages that no advance assumption of dislocation sources in simulation models is needed and they are naturally three dimensional. Farrissey et al. performed MD simulations of void growth in FCC copper and considered the effects of initial void configurations and crystal orientations [17]. Their results show that the MD simulations predict qualitatively similar deformation patterns while dramatically different stress level against the single crystal plasticity model. Seppala and his coworkers [18] investigated the effect of stress triaxiality on void growth in single crystal

* Corresponding author. Address: AML, Department of Engineering Mechanics, Tsinghua University, Beijing 100084, PR China. Tel./fax: +86 1062783488.
  E-mail address: chencq@tsinghua.edu.cn (C.Q. Chen).

copper with MD simulations. The void growth problem was examined in terms of void growth rate, void shape evolution, and stress–strain response. It was found that von Mises stress instead of mean stress plays more important role at early stages of void growth. They also studied the coalescence process by considering the growth of two voids [19]. Potirniche et al. explored the void growth and coalescence in single crystal nickel by the molecular dynamics method in conjunction with the modified embedded atom method [20]. A thin plate with either one void or two voids was modeled, showing that the plastic slip is sensitive to the specimen size and aspect ratio.

Recent laser shock experiment on nano-scaled void growth in Cu suggests that dislocation emission, rather than vacancy diffusion, is the dominant mechanism governing the growth of a void [12]. The observed strong interaction between dislocations and nano-scaled void in Cu indicates that size/scale plays an important role in void growth, similar to the experimentally characterized mechanical behavior of small scale materials and structures [21,22]. However, the macroscopic consequence of the influence of specimen size/scale on nano-sized void growth and especially its microscopic underlying mechanism is yet to be systematically clarified. The present study aims therefore to carry out MD simulations to examine in detail dislocation emission in FCC single crystal Cu containing periodically distributed nano-voids and to quantify the dependence of its macroscopic Young's modulus and yield strength upon sample size, crystalline orientation and void volume fraction.

## 2. Simulation method

Periodic unit cell model as shown in Fig. 1 is employed to study void growth in FCC single crystal copper subjected to uniaxial tension by using the MD method. The model is rendered to be representative of single crystal copper containing a periodic array of nano-voids. The uniaxial stressing loading is applied along the $x$ direction, with periodic boundary conditions enforced in the $y$ and $z$ directions where $x$, $y$ and $z$ are Cartesian coordinates. In Fig. 1, $R$ is the radius of the through-thickness circular cylindrical hole and $L_x$, $L_y$ and $L_z$ are the dimensions of the unit cell model in the $x$, $y$ and $z$ directions, respectively. The void volume fraction of the system is thus given by:

$$f_v = \frac{\pi R^2}{L_x L_y} \tag{1}$$

To investigate the crystalline orientation dependence of the MD simulation results, two orientations (i.e., [1 0 0]–[0 1 0]–[0 0 1] and [$\bar{1}$ 1 0]–[1 1 1]–[1 1 $\bar{2}$]) are considered. Note that dimensions of the model (i.e., $L_x$, $L_y$ and $L_z$) can not be chosen arbitrarily. Otherwise, periodicity of the unit cell model cannot be guaranteed. In theory,
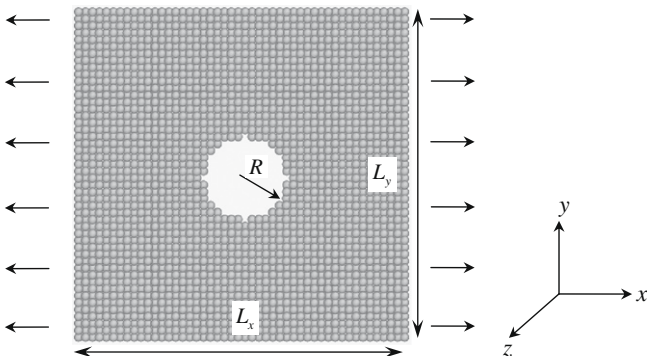


**Fig. 1.** Schematic of unit cell model for nano-voided Cu subjected to uniaxial tension in $x$ direction.

$L_x$, $L_y$ and $L_z$ must be multiple of the respective minimum periodic distance (denoted by $a_k$ with $k = x$, $y$ and $z$) which is crystalline orientation dependent. For the [1 0 0]–[0 1 0]–[0 0 1] crystalline orientation, the minimum periodic distance in the $x$, $y$ and $z$ direction is $a_k = a_0/2$ ($k = x$, $y$ and $z$) while the corresponding minimum periodic distances for the [$\bar{1}$ 1 0]–[1 1 1]–[1 1 $\bar{2}$] system are $a_x = \sqrt{2}a_{0/2}$, $a_y = \sqrt{3}a_{0/2}$ and $a_z = \sqrt{6}a_{0/2}$, respectively, where $a_0 = 0.361$ nm is the lattice constant for copper at room temperature. In addition, $L_x$, $L_y$ and $L_z$ must be greater than the potential cut-off radius $r_c$ in order to eliminate the interference from the same atom in neighboring periodic cells. In the following simulations, $L_z$ is set to be greater than four times the primitive cell length to eliminate additional size effect in the $z$ direction [23].

The interaction among the constituent atoms is described by the embedded atom method (EAM) potential proposed by Foils et al. [24]. The total energy $E$ of the atomistic system comprises summation over the atomistic aggregate of the individual embedding energy $F^i$ of atom $i$ and pair potential $\phi^{ij}$ between atom $i$ and its neighboring atom $j$,

$$E = \sum_i F^i \left( \sum_{j \neq i}^n \rho^i(r^{ij}) \right) + \frac{1}{2} \sum_{ij, i \neq j} \phi^{ij}(r^{ij}) \tag{2}$$

where the lower case Latin supercripts $i$ and $j$ refer to atoms, $r^{ij}$ is the distance between atoms $i$ and $j$, and $\rho^i$ is the electron density of atom $i$. With the total energy $E$ determined from Eq. (2), the interaction force between atoms $i$ and $j$ can be calculated as:

$$f_\alpha^{ij} = \frac{\partial E}{\partial r^{ij}} \frac{r_\alpha^{ij}}{r^{ij}} \tag{3}$$

where the Greek subscript $\alpha$ denotes the directional component. The virial formula for stress [25] is used to calculate the stress tensor for the atomistic system:

$$\sigma_{\alpha\beta} = -\frac{1}{V} \left( \sum_i \frac{p_\alpha^i p_\beta^j}{m^i} + \sum_i \sum_{j>1} r_\alpha^{ij} f_\beta^{ij} \right) \tag{4}$$

where the first term on the right hand is the kinetic contribution of atom $i$ with mass $m^i$ and momentum $p_\alpha^i$ and the second term is the microscopic virial potential stress. The stress for the atomistic system is defined as the volume average of per-atom tensor.

To avoid thermal activation, all MD simulations are performed at 0 K with the Large-scale Atomic/Molecular Massively Parallel simulator (LAMMPS) developed by Plimpton [26]. A time step of 1 fs ($10^{-15}$ s) is used to integrate the equations of motion for atoms. It should be noted that the MD simulated stress–strain responses of materials are strain rate sensitive when the applied strain rate is greater than a critical value [27]. However, strain rate sensitivity is out of current concern. The applied strain rate in the present MD simulations should be chosen within the strain rate insensitive region. It is found through trial and error that a strain rate of $2 \times 10^8$ s$^{-1}$ is a good trade-off between computational efficiency and rate insensitivity, and hence is adopted in all simulations. This value is close to those reported by Horstemeyer et al. [27] on a MD study of the shear behavior of nickel and copper, in which the critical strain rate between rate sensitive and rate insensitive regions lies in the range of $10^7 - 10^8$ s$^{-1}$.

The simulation procedure is as follows. In each of the following simulations, an atomistic unit cell model is first generated in accordance with a particular orientation and then relaxed using the conjugate gradient method to reach a minimum energy state (i.e., the ground state). Afterwards, the generated atomistic system is loaded incrementally. During each loading increment, a small strain increment of 0.1% in the $x$ direction is applied to the outermost atoms (about 5 layers of copper atoms) from both ends of the

system in the *x* direction. Right after each strain increment, the system is simulated with NPT ensemble (i.e., systems with fixed pressure *P*, temperature *T*, and number of atoms *N*) to ensure uniaxial stressing state, i.e., zero pressure in the *y* and *z* directions and uniaxial stressing in the *x* direction.

Visualization of the atomistic configurations during deformation is realized by ATOMEYE [28]. To view the evolution of defect during void growth, the centrosymmetry parameter *P* defined by Kelchner et al. [29] is employed, which has been proven to be effective for FCC crystals:

$$P = \sum_i |\mathbf{R}_i + \mathbf{R}_{i+6}|^2 \qquad (5)$$

where $\mathbf{R}_i$ and $\mathbf{R}_{i+6}$ are the vectors corresponding to the six pairs of opposite nearest atoms. The centrosymmetry parameter *P* increases from 0 for perfect FCC lattice to positive values for defects and for atoms close to free surfaces. In the case of single crystal copper, $0.5 < P < 3$, $3 < P < 16$, and $P > 16$ correspond to partial dislocations, stacking faults and surface atoms, respectively.

## 3. Results and discussion

### 3.1. Size effects

In order to explore the effect of cell size on the uniaxial stress–strain response of nano-voided single crystalline copper, unit cell models as shown in Fig. 1 with different sizes but constant void volume fraction are employed. This is achieved by fixing the ratios $R/L_x$ and $L_x/L_y$ and systematically varying the dimension $L_x$. Numer-

ical results (not shown here for brevity) show that the dimension in the *z* direction has negligible effects on the stress–strain curves, provided that $L_z$ is greater than the potential cut-off radius $r_c$ and also greater than four times the primitive cell length [23]. This is consistent with the fact that the considered nano-void is cylindrically circular and periodic boundary conditions are applied in the *z* direction. When non-periodic boundary conditions are adopted, however, significant scale size effect in the *z* direction would be expected [17].

MD calculated uniaxial stress–strain curves of [1 0 0]–[0 1 0]–[0 0 1] oriented nano-voided single crystal Cu with fixed void volume fraction of 4.9% are shown in Fig. 2a, for four selected cell sizes of $L_x/a_0 = L_y/a_0 = 24, 32, 64$, and 80. Size effect is evident in the simulated stress–strain curves (see Fig. 2a): The peak stress in the stress–strain curves increases from 5.4 to 6.9 GPa with the cell size decreasing from $L_x/a_0 = 80$ to 24, and the corresponding failure strain at the peak stress also increases with decreasing sample size. Similar feature of smaller samples behaving stronger has been reported on the shear strength of single crystal nickel and copper solids without void [27].

The peak stress in the stress–strain curves can be defined as the incipient yield strength, as explained in the following. Dependence of the incipient yield strength upon the normalized cell size ($L_x/a_0$) is summarized in Fig. 3a for two void volume fractions of 4.9% and 19.6%. Results are given for $L_x/a_0$ in the range 20 and 140. For both void volume fractions, the incipient yield strength of the smallest sample is more than 25% greater than that of the biggest sample. However, the size effect gradually diminishes when $L_x/a_0$ is greater than 120, corresponding to about 43.3 nm.
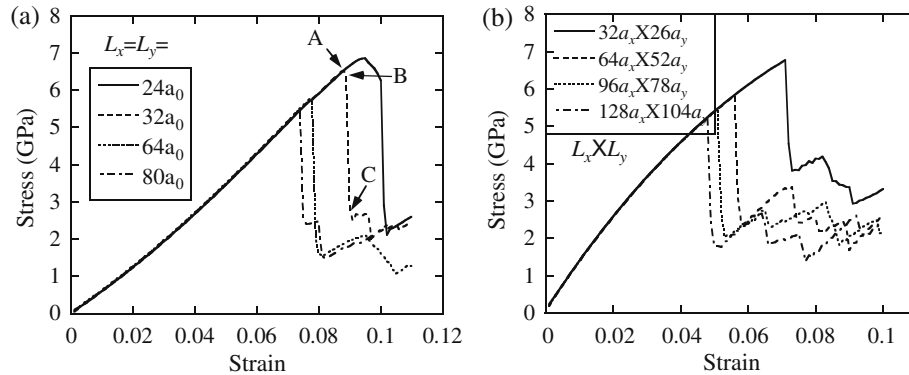


**Fig. 2.** Effect of cell size on MD simulated uniaxial stress–strain curve of single crystal Cu with circular cylindrical void of fixed void volume fraction of 4.9%: (a) [1 0 0]–[0 1 0]–[0 0 1] oriented system; (b) [$\bar{1}$ 1 0]–[1 1 1]–[1 1 $\bar{2}$] orientated system.



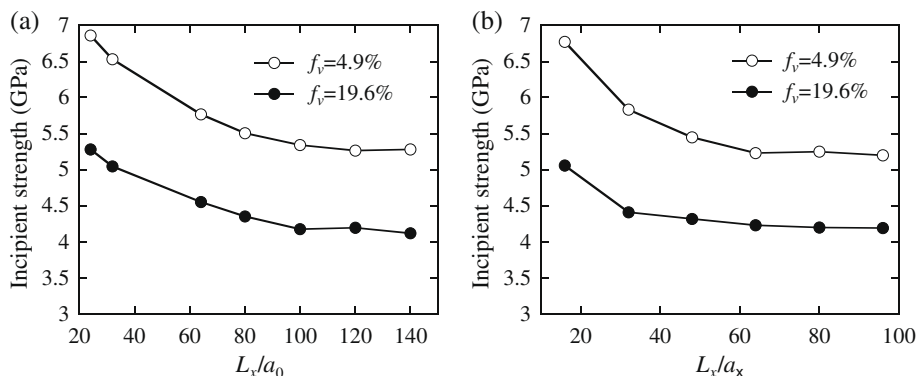**Fig. 3.** Incipient yield strength of nano-voided Cu plotted as a function of cell size: (a) [1 0 0]–[0 1 0]–[0 0 1] oriented system; (b) [$\bar{1}$ 1 0]–[1 1 1]–[1 1 $\bar{2}$] orientated system. Results are shown for two void volume fractions of 4.9% and 19.6%.

Define the initial slope of the predicted uniaxial stress–strain curves as shown in Fig. 2 as the macroscopic effective Young's modulus in the [1 0 0] direction (denoted by $\langle E_{[100]}\rangle$). The predicted influence of cell size on $\langle E_{[100]}\rangle$ is shown in Fig. 4a for the two void volume fractions of 4.9% and 19.6%. It is interesting to see from Fig. 4a that even when the cell size is as small as $L_x/a_0 \approx 20$, unlike the incipient yield strength (Fig. 3a), the macroscopic Young's modulus is almost insensitive to the cell size.

The deformation pattern accompanying the observed size effect is examined, with the defined centrosymmetry parameter (5). A sequence of three deformed atomistic configurations at strain levels indicated by A, B and C in Fig. 2a is illustrated in Fig. 5 for the sample of size $32a_0 \times 32a_0 \times 6a_0$ and void volume fraction $f_v = 4.9\%$. In Fig. 5, atoms are colored according to their centrosymmetry parameter value to give a rough picture of the defect pattern around the void. Note that Point A is at the peak of the stress–strain curve, Point B is one loading increment after the peak load, and Point C is one more loading increment after Point B. It is seen from Fig. 5a that, at the peak load point A, the centrosymmetry parameter $P$ is close to zero everywhere except for the atoms near the void surface, indicating that the atomistic system retains its near-perfect lattice structure during elastic deformation. At just one more loading increment after the peak loading, partial dislocations start to nucleate from both the top and bottom sides of the free void surface (Fig. 5b). Upon further loading, dislocations propagate across the entire sample (Fig. 5c). Therefore, the peak load points in the uniaxial stress–strain curves are associated with the initiation of partial disloca-
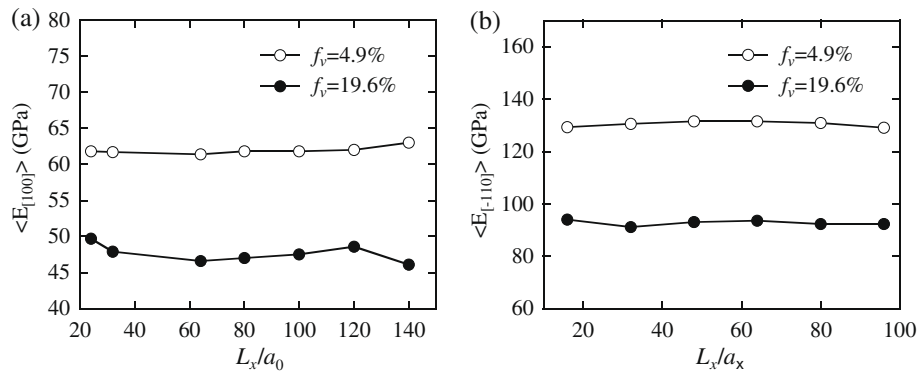


**Fig. 4.** Macroscopic effective Young's modulus of nano-voided Cu plotted as a function of cell size: (a) [1 0 0]–[0 1 0]–[0 0 1] oriented system; (b) [$\bar{1}$ 1 0]–[1 1 1]–[1 1 $\bar{2}$] orientated system. Results are shown for two void volume fractions of 4.9% and 19.6%.
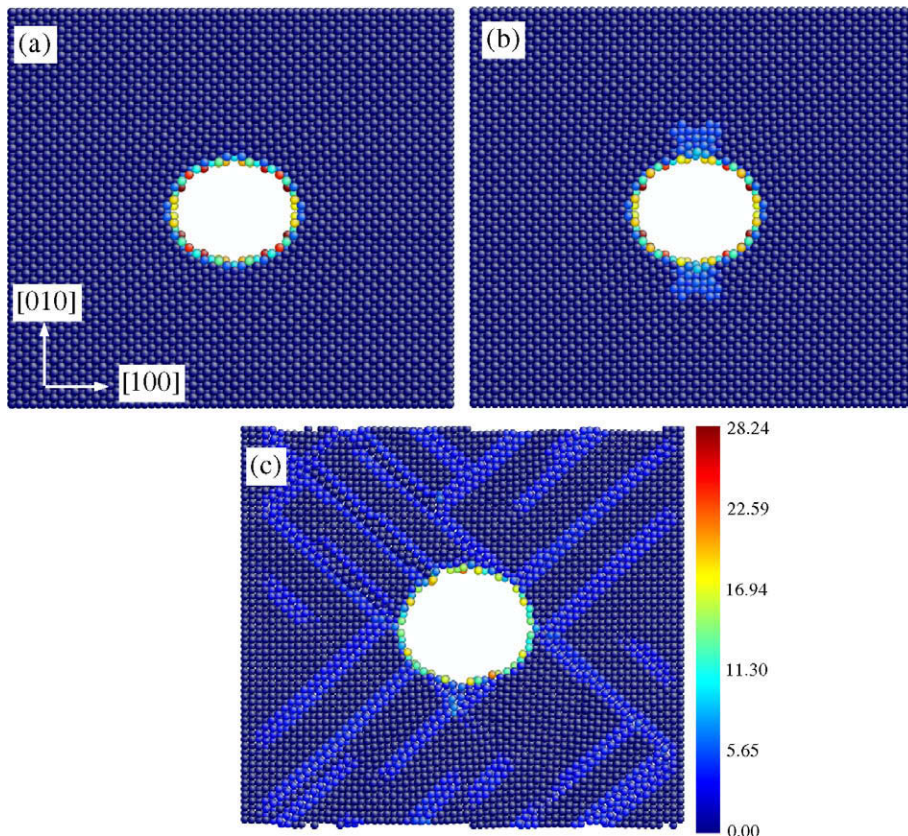


**Fig. 5.** Deformed atomistic configurations of [1 0 0]–[0 1 0]–[0 0 1] oriented sample with dimensions of $32a_0 \times 32a_0 \times 6a_0$ and void volume fraction of 4.9%. Atoms are color-coded according to their centrosymmetry parameter. Configurations (a–c) correspond to deformation states marked by A–C in Fig. 2a.

tions and are defined as the incipient yield strength of nano-voided Cu subjected to uniaxial tension.

Dramatic structural change is noted between Fig. 5b and c though the strain level of the former differs only by *one* loading increment (i.e., 0.1% in strain) from the latter. In fact, the deformation from Fig. 5b and c corresponds to a rapid and unstable process. To investigate this further, Fig. 6 presents four snapshots of atomistic configurations during the energy relaxation process between the strain loading levels of Fig. 5b and c. To show the defects in the form of partial dislocations, only atoms with their centrosym-

metry $P$ in the range of 0.5 and 3 are visible in Fig. 6. The atomistic configurations (a–d) in Fig. 6 correspond to the relaxation instances of 0, 20, 50, and 90 fs after the peak loading, respectively. It is clear from Fig. 6 that partial dislocations and dislocation loops accompany the unstable process between Fig. 5b and c. This is consistent with the experimental and atomistic studies ([12,30]) that dislocation loops emanate from nano-void in Cu. Beyond 90 fs (see Fig. 6d), the developed dislocation network swaps through the entire system and stacking fault is formed, as indicated by the light blue atoms in Fig. 5c.
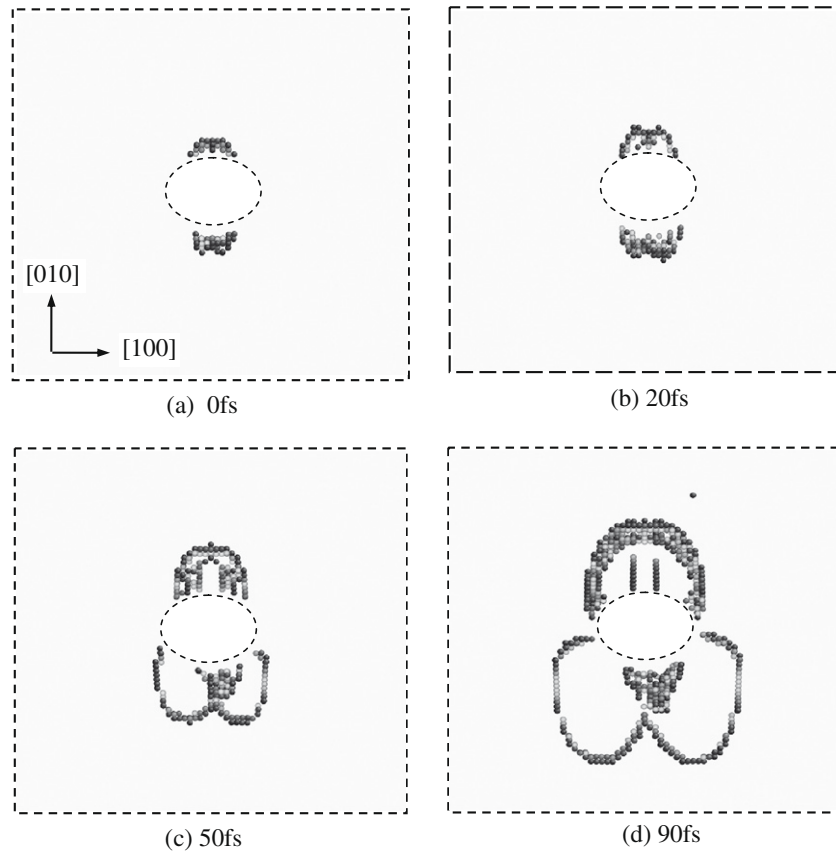


**Fig. 6.** Snapshots of atomistic configurations during relaxation process between loading levels of Fig. 4b and Fig. 4c. Only atoms with their centrosymmetry parameter in the range between 0.5 and 3 are visible to illustrate the defect in the form of partial dislocations.
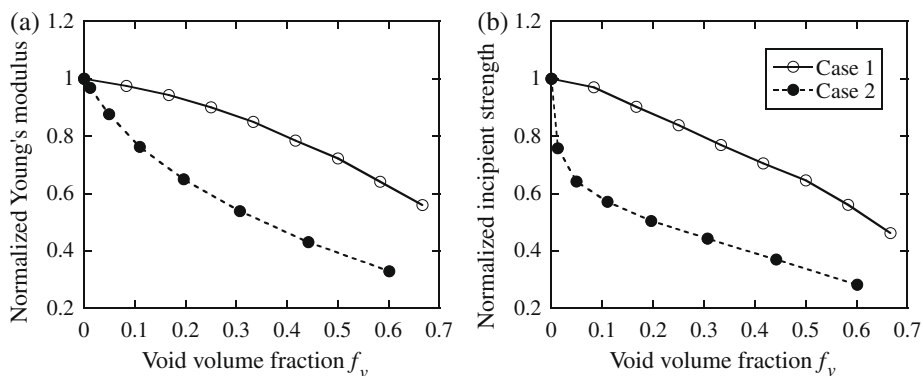


**Fig. 7.** Dependence of normalized (a) macroscopic effective Young's modulus and (b) incipient yield strength on void volume fraction for FCC single crystal Cu. Open circles:[1 0 0]–[0 1 0]–[0 0 1] orientation; solid circles: [$\bar{1}$ 1 0]–[1 1 1]–[1 1 $\bar{2}$] orientation.

## 3.2. Effects of crystalline orientation

In addition to the [1 0 0]–[0 1 0]–[0 0 1] orientation, the [$\bar{1}$ 1 0]–[1 1 1]–[1 1 $\bar{2}$] orientation is also of great interest for FCC single crystals since ‹1 1 0› and {1 1 1} are the most closely packed direction and plane, respectively. To investigate the size effect in the [$\bar{1}$ 1 0]–[1 1 1]–[1 1 $\bar{2}$] orientation, MD models with different sizes are constructed, with the uniaxial tension applied along the [$\bar{1}$ 1 0] direction and the axial direction of the cylindrical nano void oriented along the [1 1 $\bar{2}$] direction. Recall that the model dimensions (i.e., $L_x$, $L_y$ and $L_z$) must be multiple of the respective minimum atom spacing ($a_k$, $k = x$, $y$, and $z$) in the [$\bar{1}$ 1 0], [1 1 1], and [1 1 $\bar{2}$] directions. It is not possible to construct an atomistic structure having $L_x = L_y$ while at the same time ensure its periodicity in both the $x$ and $y$ directions, since $a_x \neq a_y$ for this orientation. Nevertheless, care has been taken to construct models with $L_x$ approaching $L_y$ as closely as possible, to remove additional effect arising from the different aspect ratios between models.

Parallel studies to those for [1 0 0]–[0 1 0]–[0 0 1] oriented systems are conducted for the [$\bar{1}$ 1 0]–[1 1 1]–[1 1 $\bar{2}$] systems. Fig. 2b presents the calculated uniaxial stress–strain curves for fixed void volume fraction of 4.9% and selected model dimensions: $32a_x \times 26a_y$, $64a_x \times 52a_y$, $96a_x \times 78a_y$, and $128a_x \times 104a_y$. The dimension in the $z$ direction is fixed at $8a_z$. Similar to that observed for the [1 0 0]–[0 1 0]–[0 0 1] oriented systems, examination of the atomistic configurations during void growth shows that the peak loading points in the stress–strain curves are associated with the initiation of dislocation emission. The dependence of incipient yield strength and macroscopic effective Young's modulus (denoted by ‹$E_{[\bar{1}10]}$›) on cell size are shown in Figs. 3b and 4b, respectively. It is seen from Figs. 2b, 3b and 4b that the size dependence of stress–strain response, incipient yield strength and macroscopic Young's modulus for the [$\bar{1}$ 1 0]–[1 1 1]–[1 1 $\bar{2}$] systems are qualitatively similar to that for the [1 0 0]–[0 1 0]–[0 0 1] systems.

## 3.3. Effects of void volume fraction

In previous sections, only two void volume fractions (i.e., $f_v$ = 4.9% and 19.6%) are considered. To study the effects of void volume fraction on the incipient yield strength and macroscopic Young's modulus of nano-voided single crystal Cu, MD models with different initial void volume fractions are constructed: For the [1 0 0]–[0 1 0]–[0 0 1] and [$\bar{1}$ 1 0]–[1 1 1]–[1 1 $\bar{2}$] oriented systems, sample sizes are fixed at $32a_0 \times 32a_0 \times 6a_0$ and $32a_x \times 26a_y \times 8a_z$, respectively, while the initial void radius is systematically varied. The predicted dependence of macroscopic effective Young's modulus and incipient yield strength on void volume fraction for both systems is shown in Fig. 7. Results are normalized by the corresponding Young's modulus and incipient yield strength of single crystalline Cu without void. The results of Fig. 7 demonstrate that the Young's modulus and incipient yield strength of [$\bar{1}$ 1 0]–[1 1 1]–[1 1 $\bar{2}$] oriented Cu are much more sensitive to the presence of void than those of [1 0 0]–[0 1 0]–[0 0 1] oriented Cu. For example, introduction of a nano-scaled void with 10% volume fraction leads to a decrease of 22% in Young's modulus and 42% in yield strength for [$\bar{1}$ 1 0]–[1 1 1]–[1 1 $\bar{2}$] oriented Cu while the corresponding decreases for [1 0 0]–[0 1 0]–[0 0 1] oriented Cu are only about 3.5% and 4%, respectively.

## 4. Concluding remarks

Molecular dynamics simulations have been performed to study the growth of nano-scaled circular cylindrical void in [1 0 0]–[0 1 0]–[0 0 1] and [$\bar{1}$ 1 0]–[1 1 1]–[1 1 $\bar{2}$] oriented FCC single crystal Cu subject to uniaxial tension. It is found that when the cell size is less than a threshold value (e.g., about 43 nm for [1 0 0]–[0 1 0]–[0 0 1] oriented single crystal Cu), the incipient yield strength has an apparent size dependency. Defect evolution accompanying the nano-scaled void growth has also been examined, and dislocation nucleation and emission from the free surface of the void are predicted. For the considered cell size, crystalline orientations, and void volume fraction, the predicted increase in strength due to decreasing the cell size is above 25% while negligible size effect in the macroscopic effective Young's modulus is predicted. This may have important implication for the development of macroscopic size dependent theory for void growth. For example, when incorporating the size effect into a macroscopic void growth model, it is the yield strength rather than the elastic modulus should be of greater concern.

The dependence of macroscopic effective Young's modulus and incipient yield strength upon initial void volume fraction is explored. The macroscopic effective Young's modulus and incipient yield strength of the [$\bar{1}$ 1 0]–[1 1 1]–[1 1 $\bar{2}$] oriented systems are much more sensitive to the presence of nano-sized void than those of the [1 0 0]–[0 1 0]–[0 0 1] systems.

## References

[1] F.A. McClintock, J. Appl. Mech. 35 (1968) 363.
[2] J.R. Rice, D.M. Tracey, J. Mech. Phys. Solids 17 (1969) 201.
[3] A. Needleman, J. Appl. Mech. 94 (1972) 964.
[4] A.L. Gurson, J. Eng. Mater. Technol. 99 (1977) 2.
[5] V. Tvergaard, Int. J. Fract. 17 (1981) 389.
[6] J.M. Duva, J.W. Hutchinson, Mech. Mater. 3 (1984) 41.
[7] W.M. Garrison, N.R. Moody, J. Phys. Chem. Solids 48 (1987) 1035.
[8] N.A. Fleck, J.W. Hutchinson, Adv. Appl. Mech. 33 (1997) 295.
[9] B. Liu, X. Qiu, Y. Huang, K.C. Hwang, M. Li, C. Liu, J. Mech. Phys. Solids 51 (2003) 1171.
[10] V. Tvergaard, C. Niordson, Int. J. Plasticity 20 (2004) 107.
[11] J. Wen, Y. Huang, K.C. Hwang, C. Liu, M. Li, Int. J. Plasticity 21 (2005) 381.
[12] V.A. Lubarda, M.S. Schneider, D.H. Kalantar, B.A. Remington, M.A. Meyers, Acta Mater. 52 (2004) 1397.
[13] E. Van der Giessen, A. Needleman, Model. Simul. Mater. Sci. Eng. 3 (1995) 689.
[14] M. Huang, Z.H. Li, C. Wang, Acta Mater. 55 (2007) 1387.
[15] M.I. Hussein, U. Borg, C.F. Niordson, V.S. Deshpande, J. Mech. Phys. Solids 56 (2008) 114.
[16] J. Segurado, J. Llorca, Acta Mater. 57 (2009) 1427.
[17] L. Farrissey, M. Ludwig, P.E. McHugh, S. Schmauder, Comput. Mater. Sci. 18 (2000) 102.
[18] E.T. Seppala, J. Belak, R.E. Rudd, Phys. Rev. B 69 (2004) 134101.
[19] E.T. Seppala, J. Belak, R.E. Rudd, Phys. Rev. B 71 (2005) 064112.
[20] G.P. Potirniche, M.F. Horstemeyer, G.J. Wagner, P.M. Gullett, Int. J. Plasticity 22 (2006) 257.
[21] N.A. Fleck, G.M. Muller, M.F. Ashby, J.W. Hutchinson, Acta Mater. 42 (1994) 475.
[22] W.D. Nix, H. Gao, J. Mech. Phys. Solids 446 (1998) 441.
[23] M.F. Horstemeyer, M.I. Baskes, ASME J. Eng. Mater. Technol. 121 (1999) 114.
[24] S.M. Foils, M.I. Baskes, M.S. Daw, Phys. Rev. B 33 (1986) 12.
[25] M.P. Allen, D.J. Tildesley, Computer Simulation of Liquids, Oxford University Press, Oxford, 1987.
[26] S.J. Plimpton, J. Comput. Phys. 117 (1995) 1.
[27] M.F. Horstemeyer, S.J. Plimpton, M.I. Baskes, Acta Mater. 49 (2001) 4363.
[28] J. Li, Modeling Simul. Mater. Sci. Eng. 11 (2003) 173.
[29] C.L. Kelchner, S.J. Plimpton, J.C. Hamilton, Phys. Rev. B 58 (1998) 17.
[30] L.P. Davila et al., Appl. Phys. Lett. 86 (2005) 161902.